



Efficient oil/water separation using superhydrophilic polyethersulfone electrospun nanofibrous ultrafiltration membranes

Issa Sulaiman Al-Husaini^{a,*}, Abdull Rahim Mohd Yusoff^{a,b}, Mohd Dzul Hakim Wirzal^c

^a Department of Chemistry, Faculty of Science, Universiti Teknologi Malaysia, 81310 Skudai, Johor, Malaysia

^b Centre for Sustainable Nanomaterials, Ibnu Sina Institute for Scientific and Industrial Research (ISI-SIR), Universiti Teknologi Malaysia, UTM Skudai, 81310 Johor Bahru, Malaysia

^c Chemical Engineering Department, Universiti Teknologi Petronas, Bandar Seri Iskandar, 32610 Perak, Malaysia

ARTICLE INFO

Keywords:

Electrospun nanofibrous membrane
Nanoparticles
Mechanical strength
Hot pressing technique
Anti-fouling
Synthetic oily solution

ABSTRACT

This study reports the preparation and investigations of new ultrafiltration electrospun nanofibrous membranes (ENMs) incorporated with hydrous manganese dioxide (HMO) nanoparticles (NPs) for synthetic oily solution treatment. The mechanical strength and permeation properties of typical polyethersulfone (PES)-based ENMs were enhanced in three highly potential approaches. Firstly, a dimethylformamide (DMF) dope solution was prepared with n-methyl-pyrrolidinone (NMP) as the co-solvent to facilitate inter-fiber junctions. Secondly, HMO NPs were incorporated into the ENM dope solution to enhance water production and anti-fouling resistance against oil molecules. Lastly, the resultant ENMs were subjected to a hot pressing technique (HPT) to strengthen their structure and morphological properties. The results revealed that the ENMs incorporated with HMO NPs exhibited excellent oil rejection (95.42%) and promising water flux recovery (82.47%) upon exposure to a synthetic oily solution (12,000 ppm). The HMO-incorporated PES ENMs also demonstrated a high clean water productivity of over 3380 L/m²h without sacrificing oil removal rate. Furthermore, they exhibited a low degree of flux decline owing to the improved hydrophilicity and thus reducing oil contamination. This study may serve as a basis for manufacturing high-performance and robust nanocomposite ENMs for heavy wastewater treatment.

1. Introduction

The need to develop efficient membrane filtration technologies is due to the growing water shortage issue recently [1]. Membrane separation processes are highly favorable due to their low-cost operation and high energy efficiency with high flux. On top of that, due to their environmentally-friendly nature, membranes are widely used for water purification and clarification and concentration processes [2,3]. Nevertheless, designing an adequate membrane for a specific application has become a challenge for researchers [4]. Electrospun nanofibrous membranes (ENMs) are in huge demand due to their intrinsic properties such as huge surface area, high porosity, tuneability, the interconnectedness of more open-pore structure and controllable thickness [5–9]. The ENMs' porous structure could be formed using the entanglement of interconnected nanofibers, which is the space between fibers [10]. The desired pore size can be obtained by optimizing the fiber diameter depending on the filtration requirements. The advantages of ENMs include high water permeability, high porosity and good

separability owing to their highly twisted structure and the static charge in the nanofibers after electrospinning [11,12]. Moreover, ENMs are less expensive than commercial membranes (~20 vs. 50 V/m²) [13].

Ultrafiltration (UF) is a promising approach in wastewater treatment and reclamation processes, including sedimentation coagulation and sand filtration [1], because of its simple operation, low maintenance and sludge production [14]. In addition, UF-based ENMs have been widely used in air filtration, particularly microparticle removal [15]. Nevertheless, UF-based ENMs have low mechanical strength, are difficult to be handled after electrospinning [16–18]. In addition, they are highly prone to compaction, resulting in low permeability at high-pressure water filtration [19,20]. As materials with highly porous structures, ENMs have extensive stress distribution [21]. Compaction occurs within large pores and microvoids [22]. Microvoids decrease in size with pressure, increased tortuosity and decreased membrane flux [21,22]. Therefore, they are highly susceptible to rapid fouling, which can considerably decrease water production rates, affect separation performance and increase energy consumption [1,23]. In addition, the low

* Correspondence to: Sultan Qaboos University, PO Box 17, PC 123, SQU, Al-Khouth, Oman.
E-mail address: abu_mohamad76@yahoo.com (I.S. Al-Husaini).

<https://doi.org/10.1016/j.jece.2022.108341>

Received 25 February 2022; Received in revised form 21 June 2022; Accepted 25 July 2022

Available online 26 July 2022

2213-3437/© 2022 Elsevier Ltd. All rights reserved.

compaction resistance of UF-based ENMs and water treatment filters limit the development of sustainable and energy-efficient membranes [22]. Therefore, given their impact on fouling control, membrane properties and effects must be understood to develop efficient membranes. For instance, membrane properties, such as roughness, hydrophobicity, pore size and morphology, can greatly influence membrane–foulant interactions and fouling effects [1,11]. Polyethersulfone (PES) has been widely used for commercial microfiltration (MF) and UF membranes because of its high thermal and chemical resistance [19]. However, it was found that the hydrophobic character of PES-based membranes makes them suboptimal for separating water from the mixtures of oil/water and vulnerable to fouling. Sequentially, it influences the membrane water flux stability and durability.

The present study enhanced the mechanical properties and oil anti-fouling resistance of PES-based UF ENMs for oily solution treatment using innovative and practical strategies. The characteristics of UF-based ENMs were improved in three approaches. Firstly, PES-doped solutions were prepared using a mixed dimethylformamide (DMF)/N-methyl-pyrrolidinone (NMP) solvent to produce interconnected fibers during electrospinning. The combination of NMP and DMF is expected to enhance the mechanical efficiency of ENMs. NMP features high viscosity and high solubility in PES; however, the low volatility of NMP makes this solvent unsuitable for electrospinning [19]. Fortunately, the intense volatility can be mitigated through ENM wetted process, in which the remaining solvent will be removed to induce fiber solidification [16]. Secondly, the host polymer PES was modified by incorporating commercialized hydrous manganese oxide (HMO) NPs with large -OH groups into the PES membrane to alter its wetting properties from hydrophobic to hydrophilic [19,24,25]. The incorporation of hydrophilic HMO NPs into PES is expected to improve the ENM water flux and reduce the fouling issue of UF in oily wastewater filtration.

Ismail et al. [24] proved that the presence of HMO NPs with the loading of 3, 5, 7, and 10 wt% improved the hydrophilicity and oleophobicity of the PVDF membrane by reducing the water contact angle from 99° to 58° while the oil contact angle increased from 0° to 35°. Most importantly, the PVDF membrane containing 10 wt% of HMO loading exhibited 10 times greater water flux (402 L/m² h) than the pristine PVDF membrane with a 93% oil rejection rate. Al-Husaini et al. [19] incorporated 3.0 wt% of HMPO NPs into ENM which exhibited excellent oil rejection (97.98% and 94.04%) and a promising water flux recovery (89.29% and 71.10%) with water productivity of over 7000 L/m² h for treatment of synthetic oily solution (5000 or 10,000 ppm oil), respectively. Furthermore, Lai et al. [26] reported that incorporating different ratios of HMO and titanium dioxide (TiO₂) nanoparticles into asymmetric PSF membrane leads to 31.73% and 26.41% higher water flux compared to the neat PES membrane due to increment in membrane surface hydrophilicity. Moreover, the nanofillers-incorporated membranes showed a significantly lower degree of flux decline due to improved surface resistance against oil fouling and potential for long-term operation with an extended lifespan. Meanwhile, Gohari et al. [25] studied that HMO NPs successfully improve the PES membrane surface hydrophilicity by reducing the contact angle from 69.5° (in the neat PES) to less than 16.5° (in the HMO-modified membrane) which, resulted in remarkable enhancement in water permeability (up to 573.2 L/m²h bar) with excellent oil rejection (almost 100%) and a promising water flux recovery (75.4%) for treatment of 1000 ppm of synthetic oily solution. Lastly, the resultant ENMs were subjected to the HPT at 100–210 °C and 1 bar to increase their interfacial stability. HPT, aside from being more environmentally friendly and less energy-consuming than plasticizing, allows the bonding of fibers at junction points by welding the nanofibers together [1].

To the best of our knowledge, the implementation of UF-based ENMs via three approaches using mixtures of DMF/NMP solvents and the combination of hydrophilic HMO NPs into the ENMs dope solution with the hot-pressing technique for the treatment of oily industrial effluent has not been reported yet in any of the open literature. Therefore, this

study may serve as a basis for manufacturing high-performance and robust nanocomposite ENMs for heavy wastewater treatment without rigorous flux declination. The structural and morphological properties of the membranes were characterized using X-ray diffraction (XRD), Fourier-transform infrared spectroscopy (FTIR), thermo-gravimetric analysis (TGA), transmission electron microscopy (TEM), field-emission scanning electron microscopy (FESEM), energy-dispersive X-ray spectroscopy (EDS), tensile testing and water contact angle (WCA) analysis. These properties influence the filtration performance of membranes and thus are crucial to investigate. The resulting ENMs incorporated with HMO were assessed in terms of pure water flux, oil rejection and water flux recovery via the cross-flow UF system with a constant flow rate of 1 L/min.

2. Materials and methods

2.1. Materials

Pellets of polyethersulfone (PES) Ultrason E6020P (Mw: 58,000 g/mol and the density of 1.37 g/cm³) obtained from BASF (Germany) were used as the main membrane-forming material. PES pellets were dissolved in mixed DMF and NMP solvents (99% purity, Merck, Germany). In addition, polyvinylpyrrolidone (PVP, Mw:29,000 g/mol, Sigma Aldrich) and inorganic hydrophilic HMO powder (mean particle size: ~5.7 nm; Research Nanomaterials, Inc., USA) were utilized as additives to improve membrane properties. A crude oil sample was obtained from Terengganu Crude Oil Terminal, Malaysia (Location: RE110). The surfactant used in this study was sodium dodecyl benzenesulfonate (SDS, M_w: 288.4 g/mol) from Merck to stabilize the oil/water emulsion. Deionized (DI) water (ultrapure Milli-Q water) with a resistivity of 18.2 MΩ cm was utilized for sample preparation and membrane tests throughout the experiments (Millipore, USA).

2.2. Fabrication of ENMs

2.2.1. Dope solution preparation

The blended ENM/NP dope solutions were obtained through a three-step process displayed in Fig. 1. Firstly, 3 wt% HMO NPs (PES polymer weight) were introduced in the mixed DMF/NMP (50:50 wt%) solvents. The NPs were magnetically stirred overnight at 60 °C, 300 rpm. Secondly, the NP dope solution was added with 0.5 g of PVP. The resulting mixture was stirred at 60 °C, 300 rpm until a clear homogeneous solution was obtained. Subsequently, dry PES pellets (26 g) were slowly added into the resultant mixture with stirring at 60 °C, 500 rpm for 24 h until all the pellets were completely dissolved. Before electrospinning, the obtained mixture was subjected to ultra-sonication (40 kHz, 25 °C) for 3 h to eliminate air bubbles trapped inside the container. The dope solution for a pure PES membrane was obtained without PVP or HMO compared with the ENMs/PVP and ENMs/NPs. The electrical conductivity and viscosity of the solutions were measured with an EC meter (Eutech CON 700, Singapore) and a viscometer (Brookfield, DV2T, USA), respectively. The results are summarised in Table S1.

2.2.2. Membrane fabrication

ENMs were manufactured using Inovenso's (Turkey) electrospinning technology (Fig. 1(b)). The dope solution was placed inside a syringe pump (BD, USA) with a rocket metal single nozzle (øID = 0.37 mm). Different injection rates (0.8 mL/h followed by 0.5 mL/h and 0.3 mL/h with 3 h intervals) were used to alter the pore structure and improve the permeability of the nanofiber mats. The optimum conditions of the ENMs are as follows: collector rotation speed of 350 rpm, Ø 7 cm; nozzle tip and collector distance of 12.8–14.6 cm, and voltage of 26.2 kV. The process was conducted at a constant temperature (25 ± 2 °C) and relative humidity of 55% ± 5%. The ENMs were collected on a drum collector covered with aluminum foil.

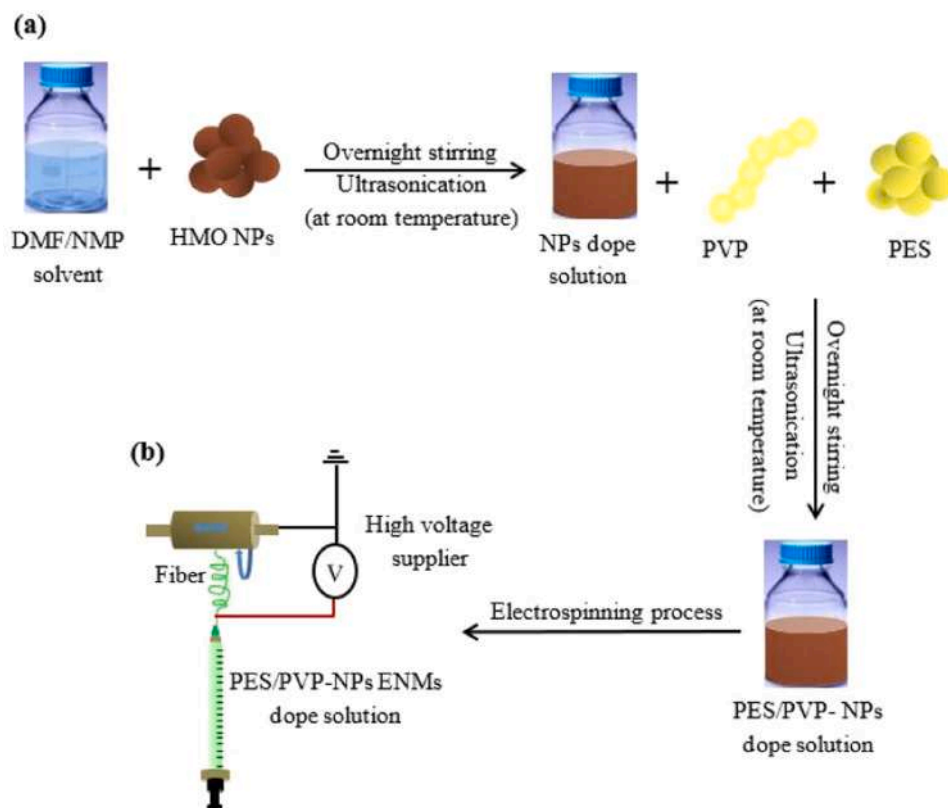


Fig. 1. (a) preparation of PES/PVP-NPs dope solution and (b) electrospinning set-up for ENMs fabrication.

2.2.3. Post-treatment of the ENMs

The ENMs were treated using two methods. The membrane was immersed in a deionized (DI) water bath for 3 days in the first method. DI water was changed daily to remove the remaining solvents completely and avoid the agglomeration of the PVP and NPs from the nanofiber membranes before use. Next, the membranes were washed thoroughly with DI water before being allowed to dry between filter papers at room temperature (RT) for 24 h. Finally, the ENM was oven-dried for 24 h at 65 °C [27,28] and then in a desiccator cabinet (Secador, USA) at RT (with a humidity between 10% and 20%) for further treatment. In the second method, ENMs were subjected to HPT using a hydraulic-press system (Motor Hydraulic Lab Press) [23,29] to improve their interfacial properties, as shown in Fig. S1. Initially, the ENMs were trimmed with plates to minimize contamination, placed in the hydraulic-press system and then pressed for 10 min at 1 bar at different temperatures of 100, 160, and 210 °C.

2.3. ENM characterizations

2.3.1. Morphological characterizations

The surface morphology of the ENMs was explored via FESEM (JEOL JSM-7600F, Japan). The surface of the material was coated with a conductive layer of platinum (Pt) using a K575x coater (JEOL JFC-1600, Japan) [25]. The fiber diameter distribution was studied using ImageJ (NIH, USA). An average of 65 nanofibrous diameters was measured from the FESEM images. Five casual points on the top layer were selected and averaged to measure the thickness of the top-layered cross-sectional ENMs. The energy-dispersive X-ray spectroscope (EDS) was used to detect the elemental ratio of the ENMs samples. Five different positions were selected, and the mean was calculated.

The duplicate solution was electrospun directly on a copper grid (carbon films, 200-mesh grid, AGAR) for approximately 12 s. TEM images of the NPs were then obtained with a JEOL JEM-2100F by dispersing the NPs in ethanol and sonicating for 45 min to ensure the

formation of a homogeneous suspension. A droplet of this suspension was placed on the copper grid before placing it in a dry pumping station at 60 °C for 1 h. The particle size of HMO was estimated using Digital Micrograph (Gatan Software Version 3.x).

The pore size distribution of ENMs was determined using a mercury intrusion pore size analyzer (PoreMaster-60 GT, Anton Paar, USA). The ENMs samples were cut and folded into small pieces to prior inserting into the penetrometer. Each sample was measured three times, and the average value was obtained.

The porosity percentage ($\epsilon\%$) of the ENMs was calculated using Eq. (1) based on the subtraction of the weight of the membrane in wet (W_w) and dry (W_d) states [30]:

$$\epsilon(\%) = \left(\frac{\frac{(W_w - W_d)}{\rho_{H_2O}}}{\frac{(W_w - W_d)}{\rho_{H_2O}} + \frac{W_d}{\rho_{PES}}} \right) \times 100 \quad (1)$$

where ρ_{H_2O} is the pure water density (0.998 g/cm³), and ρ_{PES} is the density of PES (1.37 g/cm³).

2.3.2. Structural characterizations

FTIR spectroscopy was performed on a Paragon 1000 Spectrometer (PerkinElmer, USA) at 500–3500 cm⁻¹. Each sample was scanned 32 times with a resolution of 4 cm⁻¹, and the samples were prepared using KBr pellets.

The XRD profiles of the NPs and ENMs were determined on a XRD diffractogram (MiniFlex 6000, Rigaku, Japan) equipped with Ni-filtered Cu-K α radiation ($\lambda = 1.54056 \text{ \AA}$) and operated at 40 mA and 40 kV. XRD analysis was conducted at a scan rate of 2°/min and a step size of 0.01° with a diffraction angle 2θ range of 10–90°.

The thermal behaviour of the ENMs and NPs was analyzed using PerkinElmer Pyris STA 6000. Approximately 10–30 mg of each sample was heated from 30 °C to 990 °C at a heating rate of 10 °C/min in a

nitrogen gas atmosphere and a 20 mL/min flow rate.

2.3.3. Tensile testing

The mechanical properties of the ENMs were analyzed on an Instron Microtester tensile testing machine with a load limit of 1000 N (HT400, USA) according to ASTM D882–10 standard. Each sample was sectioned into rectangular strips with 4 cm (W) × 3 cm (L). The crosshead speed of 20 mm/min and the gauge length of 20 mm were used. At least five measurements were taken, and the average for each sample was reported. The tensile strength (MPa) and the elongation at break (%) were determined based on the resultant stress versus strain plot (obtained from load-elongation data) [27].

2.3.4. Water contact angle

The hydrophilic propensity of the ENM sample was evaluated using an optical contact angle analyzer (FI-02130 Espoo, Finland). Milli-Q water (5 mL) served as the probe liquid. Images of WCA on the sample surface were obtained using a digital camera. Data were collected from at least five locations.

2.4. Filtration study

2.4.1. Synthetic oily solution

The synthetic oily solution was prepared by mixing crude oil (medium oils) at a concentration of 12,000 ppm with DI water following the method reported by Lai et al. [26] and Gohari et al. [25]. The solution was mixed with sodium dodecyl benzenesulfonate (SDS) to solubilize the crude oil in DI water and form a stable oil-in-water emulsion as previously described by Al-Husaini et al. [23]. The ratio of crude oil to SDS was set at 9:1 (w/w), as reported by Lai et al. [26]. Then, the crude oil-in-water emulsion was stirred vigorously at 500 rpm for about 45 min at room temperature using a mechanical blender (BL 310AW, Khind) to produce a solution with a uniformly yellowish color. The synthetic oily solution (12,000 ppm) was used during the filtration of ENMs to confirm that the proposed ENMs are beneficial for treating diverse industrial oily solution discharge without rigorous flux declination.

2.4.2. Sizes of oil droplets measurement

The particle sizes of the oil droplets were measured using a Zetasizer

Nano ZSP (Malvern Instrument Inc., UK). The refractive indexes of the oil droplets and dispersant (water) were set at 1.59 and 1.330, respectively.

2.4.3. Ultrafiltration system and operating parameters

A laboratory-scale cross-flow UF system fabricated with a permeation cell with a surface area of the membrane of 24.63 cm² was used to measure the permeation flux of pure water and the oil rejection (R) of the prepared ENMs. Fig. 2 shows a schematic diagram of the cross-flow UF system.

The ENMs were wetted with deionized water in advance before running the permeation test. Then, the ENMs were placed inside the permeation cell. The solution in the storage solution container was flowed on the top part of the membrane surface with a peristaltic pump (77200–60, Masterflex L/S, Cole Parmer) at a flow rate of approximately 1 L/min during the entire test time (Fig. 2). The filtrate side and the feed solution were not subjected to any pressure. The flux was determined by measuring the amount of permeate collected in the measuring cylinder (50 mL). Each respective ENM was tested at least three times to obtain the average value of permeate fluxes.

2.4.4. Pure water permeation flux and oil rejection (R_{oil} , %) experiments

UF test of the ENMs was performed for pure water flow before exposure to the synthetic oily solution. The purified water from the analyzed sample was withdrawn from the permeate every 15 min for 120 min, and the remaining permeate was returned to the tank. The produced retentate flow was measured using a flow meter. The pure water flow (J_{w1}) through the membrane was calculated using Eq. (2) as described by Liu et al. [31]:

$$J_{w1} = \frac{V}{A \times t} \quad (2)$$

where J_{w1} is the water permeation flux of membrane (L/m² h), V is permeated pure water volume (L), A is the membrane surface area (m²), and t is the permeate collection time (h). Similarly, the permeate pure water flux (J_{w2}) of the ENMs treated with the synthetic oily solution was calculated. The membranes performance was evaluated using an artificial oily solution of 12,000 ppm as feed solution. The oil rejection (R_{oil} %) of the membranes was obtained using Eq. (3) as reported in the literature [31,32]:

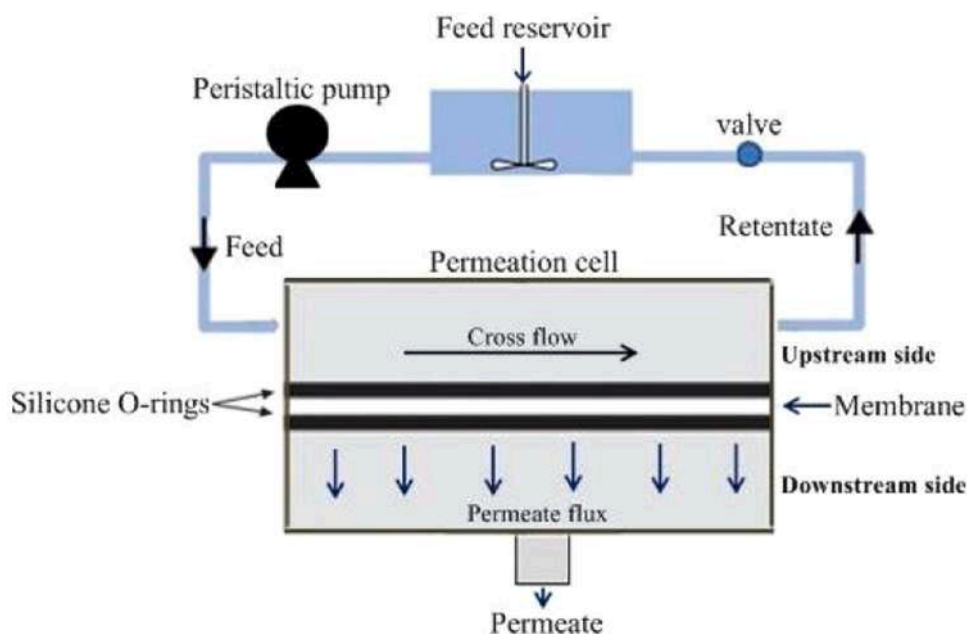


Fig. 2. Schematic diagram of the cross-flow UF arrangements (the hues have no significance).

$$R_{oil}\% = \frac{C_{oil,F} - C_{oil,P}}{C_{oil,F}} \times 100 \quad (3)$$

where $C_{oil,F}$ and $C_{oil,P}$ are the respective oil content (mg/L) of UF-ENMs in the feed and permeate solution.

2.4.5. Oil content measurement

Feed and permeate samples were collected in every experiment at 20 min intervals (each sample was tested three times) to approximate the oil content of the membrane permeate flow and the oil rejection. A UV-vis spectrophotometer (DR5000, Hach, USA) was used to determine the oil concentrations in the feed and permeate samples. The filtration experiment was conducted for 120 min to examine the properties of the

ENMs. The calibration curve obtained from pattern solutions at 280 nm was used to evaluate the rejection efficiency of the ENMs. The flux decline was normalized to water flux (J_i/J_o), as previously described by Lai et al. [26].

2.4.6. Flux recovery ratio measurement

The ENMs surface was hydraulically cleaned after being treated with an oily solution using DI water flow (two times for 30 min). The membranes' flow recovery rate (R_{FR}) was determined by replacing the feed solution tank and replenishing it with water. Each membrane sample was tested three times, and the mean was calculated together. R_{FR} was obtained by re-evaluating the pure water flux of the cleaned ENMs (J_{W_2}) using Eq. (4) as reported by Lai et al. [26]:

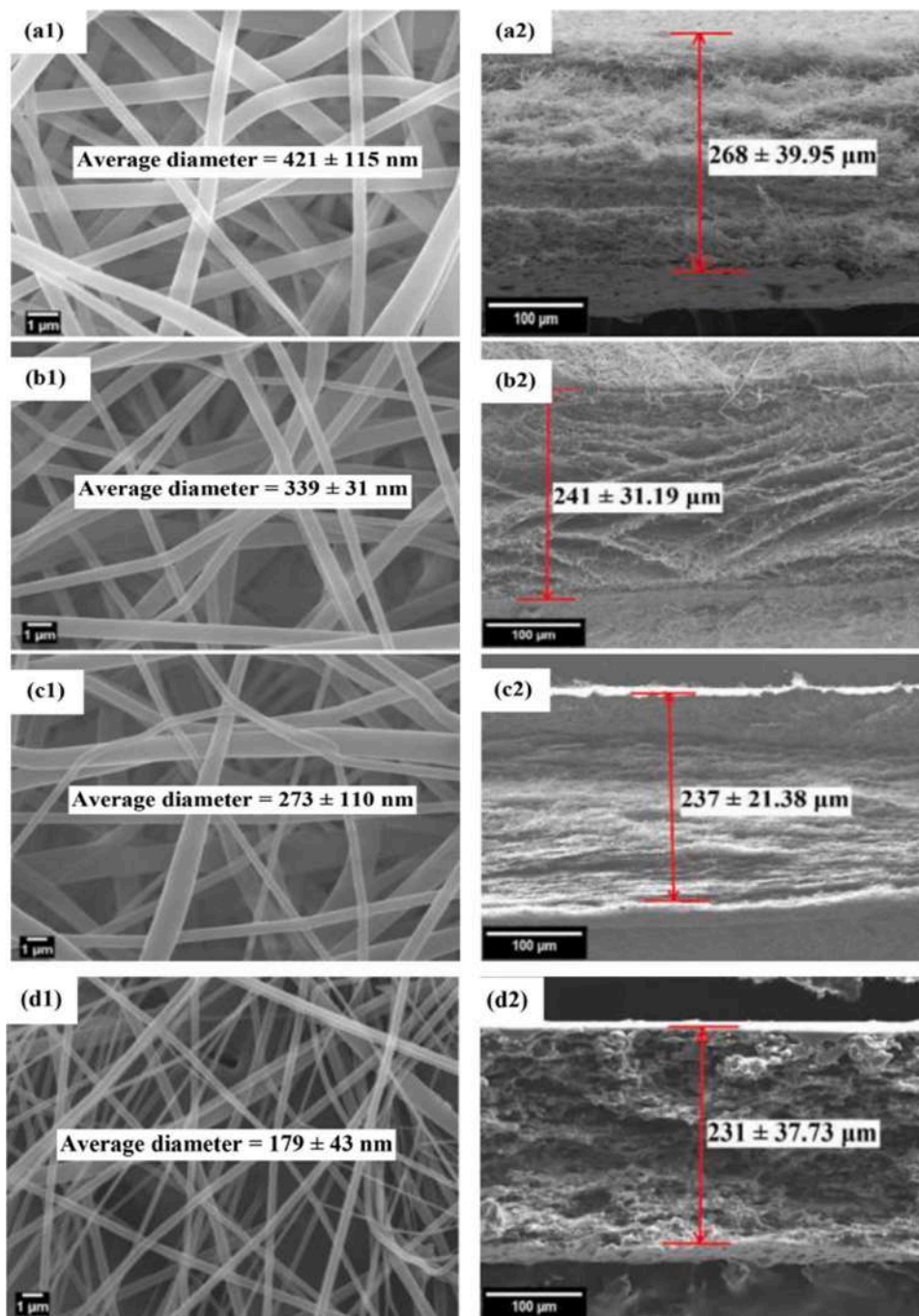


Fig. 3. FESEM images of the (left: top surface view at a magnification of 5000x and right: cross-sectional view, 170x) of (a) pure PES, hot-pressed (b) PES, (c) PES/PVP, and (d) PES/HMO ENMs.

$$R_{FR}(\%) = \left(\frac{J_{w2}}{J_{w1}} \right) \times 100 \quad (4)$$

3. Results and discussion

3.1. ENMs properties

3.1.1. Morphological properties

Previous studies applied HPT via pressure and heat to improve the fiber connectivity and membrane intersection for separating oil and water emulsions. Ahmed et al. [33] reported that upon application of HPT, the morphology of electrospun polyvinylidene fluoride-co-hexafluoropropylene (PVDF-HFP) and cellulose/electrospun PVDF-HFP composite membranes were improved as both hot pressing ENMs were merged at the intersecting sites. This interlocking of fibers resulted in excellent oil removal efficiencies up to 99.98% with superior mechanical stability. Tan et al. [34] applied HPT onto TiO₂/Fe₂O₃ composite membrane at 5 bar and 100 °C which resulted in outstanding anti-oil fouling and self-cleaning properties. Due to the remarkable and excellent advantages of HPT application, this post-treatment method was employed in this work to strengthen the electrospun mat and prevent delamination of the nanofibrous layer during the liquid filtration process. Our results showed that the ENMs hot-pressed at 100 °C and 160 °C exhibited unfavorable structure, not adhering completely. Therefore, higher hot pressing temperatures (210 °C) study was carried out on the ENMs. The selected temperature for the heat treatment (210 °C) is above the boiling point of the solvents (DMF = 153 °C and NMP = 202 °C) and below the glass transition temperature of PES (225 °C). The residual solvent in the ENMs can partially re-dissolve PES during hot pressing. Continuous heating led to strong solvent diffusion into the nanofiber surface. By evaporation of the solvent at the interface, the nanofibrous stick to each other firmly. The improved adhesion at the interface is seen in FESEM pictures (Fig. S1) as HPT was applied to the electrospun nanofibrous mat.

Fig. 3 presents the FESEM micrographs of the top surface morphology (a1–d1) and the cross-sectional view (a2–d2) of the prepared ENMs. The ENMs have fairly regular and smooth surfaces as shown in Fig. 3 (a1–d1). Compared with pure PES membrane (Fig. 3 (a1)), HPT can reduce the fiber diameter (Fig. 3 (b1)) because the compaction under heat conditions changes the morphology of the nanofibers, as shown in Fig. S1. As HPT is applied, the electrospun fibers merge at intersecting sites (Fig. S1.), allowing the fibrous structure to be more compact [6,11,33]. This results in reduced fiber diameter and enhanced mechanical stability. It was reported by Al-Husaini et al. [19] that HPT reduces the fiber diameter of pure PES membrane from 480 nm to 405 nm. According to Homaeigohar et al. [27] also heat treatment caused a reduction in the fiber diameter of a pristine PES membrane. The previous results can be attributed to the heat treatment process that helps to fuse the fibers, making the structure more compact and reducing the fiber diameter. Moreover, by comparing the hot-pressed ENMs modified by PVP (Fig. 3 (c1)) and HMO (Fig. 3 (d1)), it was found that both ENMs display significantly smaller fiber diameters (47% reduction) compared to the hot-pressed PES ENMs. This result can be ascribed to the (1) the high conductivity (Table S1), (2) the inclusion of well-dispersed HMO in the polymer dope solution, and (3) the application of heat treatment that forces the membrane morphology to change [23]. Therefore, the ENMs' doped solution conductivities (i.e., charge density) assist in the jet formation from the Taylor cone and resulted in the whipping instability of the electrospun fibers. The charge density distribution overcomes the tangential electric field along the surface of the solution droplet as the conductivity increases. Henceforth, higher solution conductivities resulted in smaller fiber diameters, whereas lower values generate larger electrospun-fiber diameters [35]. Furthermore, appropriate dispersion of NPs in the polymeric network matrix was vital to ensure superior load transport from the polymer to

the NPs. This will result in the viscosity reduction of the PES/NPs blend solution (Table S1), improving the mechanical properties. It is worth noting that although these NPs were tiny, no agglomeration had occurred, revealing their uniform dispersion over the whole surface (cross-section view), as shown in Fig. 3 (a2–d2).

Fig. 3 (a2–d2) compares the thickness (based on the cross-sectional FESEM images) of the PES-based membranes with and without HPT. The hot-pressed membranes have relatively thinner cross-sectional structures than the pristine PES membranes. The membrane thickness of the pristine nanofibrous membrane changed approximately 10.07% to the hot-pressed samples as it underwent pressure and temperature. Moreover, the hot-pressed treated ENMs displayed similar layer thicknesses (ranging from 231 and 241 μm) due to fiber fusion, promoting membrane compaction (Fig. S1). However, the variation of the morphology of ENMs highly depends on the doping solution used for membrane fabrication. As shown in Fig. 3 (d2), the average thickness obtained from the cross-sectional SEM images decreased when the PVP and NPs were incorporated. Therefore, the membrane became thinner after HPT and upon the addition of PVP and NPs. This is due to the slow evaporation of NMP in the mixed solvent in doping solution (during electrospinning) which causes the fibers to be relatively 'wet' and resulted in a slight fusion between the contacts of inter-fibers [28]. Apart from that, the incorporation of hydrophilic additives (NPs) create migrating ions in solution that transport charges hence resulting in higher conductivities of doped solution. This later produced membranes with smaller fiber diameters and thinner morphology than the other doped solution without additives [36,37].

Fig. 4(a–d) illustrates the EDS spectra of the as-synthesized ENMs. The carbon content was insignificantly decreased in the hot pressed ENMs in comparison with the pristine ENMs, as shown in Fig. 4(a) and (b). This can be explained by the evaporation of the organic solvent due to high temperature and polymer decomposition when subjected to the HP treatment. The successful integration and uniform dispersions of HMO NPs within the fibers network were further verified by Mn peaks in the EDS spectrum of PES/HMO ENMs, as shown in Fig. 4(d). The peaks at 0.64 and 5.9 KeV were due to Mn. These peaks with a slight difference in intensity suggested the embedment of HMO in the PES membrane matrix [25].

HR-TEM micrographs of the synthesized HMO NPs and hot-pressed PES/HMO nanofibrous membranes are presented in Fig. 5(a) and (b) at different scales. The synthesized HMO NPs (Fig. 5(a)) showed various flake- and needle-like microstructures with mean particle diameters below 6 nm [19,26,38,39]. The TEM images (Fig. 5(b)) clearly illustrated the morphological properties of the hot-pressed PES/HMO membrane. The TEM micrographs manifested the existence of HMO NPs in the nanofibrous membranes, and the mean particle size was ~5.7 nm (result not shown). Moreover, hot-pressed processing minimized NP aggregation, thereby achieving the excellent uniform dispersion of NPs. The chemical bonding between the HMO and sulfone/ether groups of PES may also explain the superior NP distribution without severe agglomeration, as reported by Al-Husaini et al. [19]. The inclusion of NPs on the nanofibers was verified using TEM-EDS. Fig. S2 shows the EDS spectra of the ENMs. The EDS-SEM image in Fig. 4 shows peaks at 0.64 and 5.9 KeV assigned to Mn. Nevertheless, again, these results further verified the inclusion of NP in the fabricated ENMs.

3.1.2. Structural properties

XRD profiles of the HMO NPs and the hot-pressed PES membranes incorporated with and without HMO NPs are displayed in Fig. 5(c). The HMO NPs exhibited three characteristic weak and broad peaks at 2θ values of 25.06°, 37.34° and 66.61°, which can be ascribed to the typical microcrystallinity and amorphous phases of HMO NPs. The observed peaks were comparable to synthetic birnessite phase *d*-MnO₂ [25,38]. This result suggests that the synthesized HMO NPs were in the glassy phase [19,25,38]. The XRD patterns of ENMs without and with HMO inclusion were compared. The peaks of the HMO NPs were slightly wider

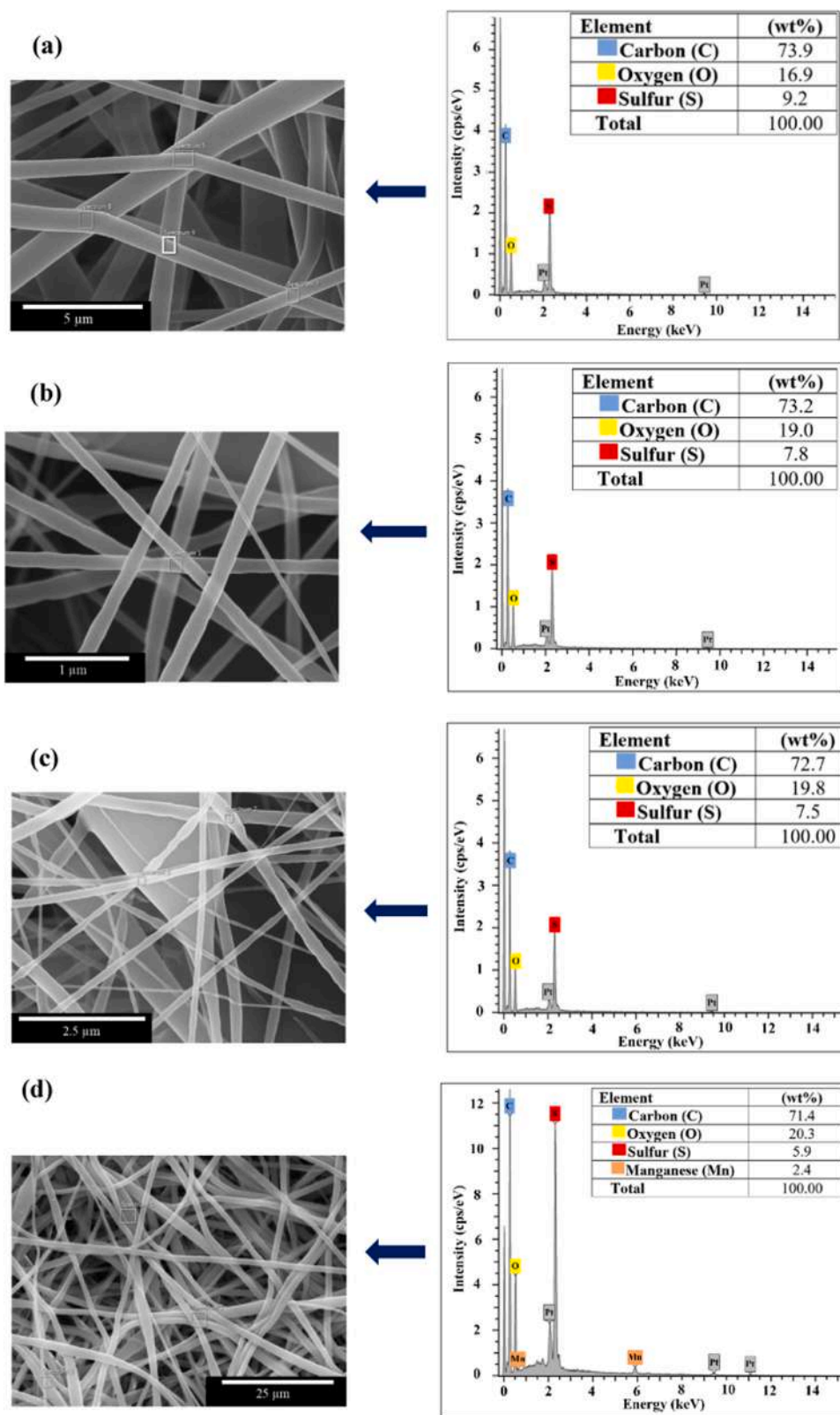


Fig. 4. FESEM images (left) and EDS spectra (right) (a) pure PES, (b) hot-pressed PES, (c) hot-pressed PES/PVP, and (d) hot-pressed PES/HMO ENMs.

after being incorporated into the PES membrane [25]. The three significant peaks of HMO further proved the successful embedment of NPs in the nanofibrous matrix. Meanwhile, such peaks were not exhibited by the hot-pressed PES nanofibrous membrane. In general, the HMO NPs formed in the hot-pressed PES nanofibrous membranes were in the

glassy phase.

Fig. 5(d) compares the FTIR spectra of the hot-pressed PES ENMs with and without HMO NPs. The broadband at 1623 cm^{-1} corresponded to the O–H bending vibration combined with the Mn atom (Mn–OH). The $400\text{--}900\text{ cm}^{-1}$ bands resulted from MnO_6 octahedra in the HMO

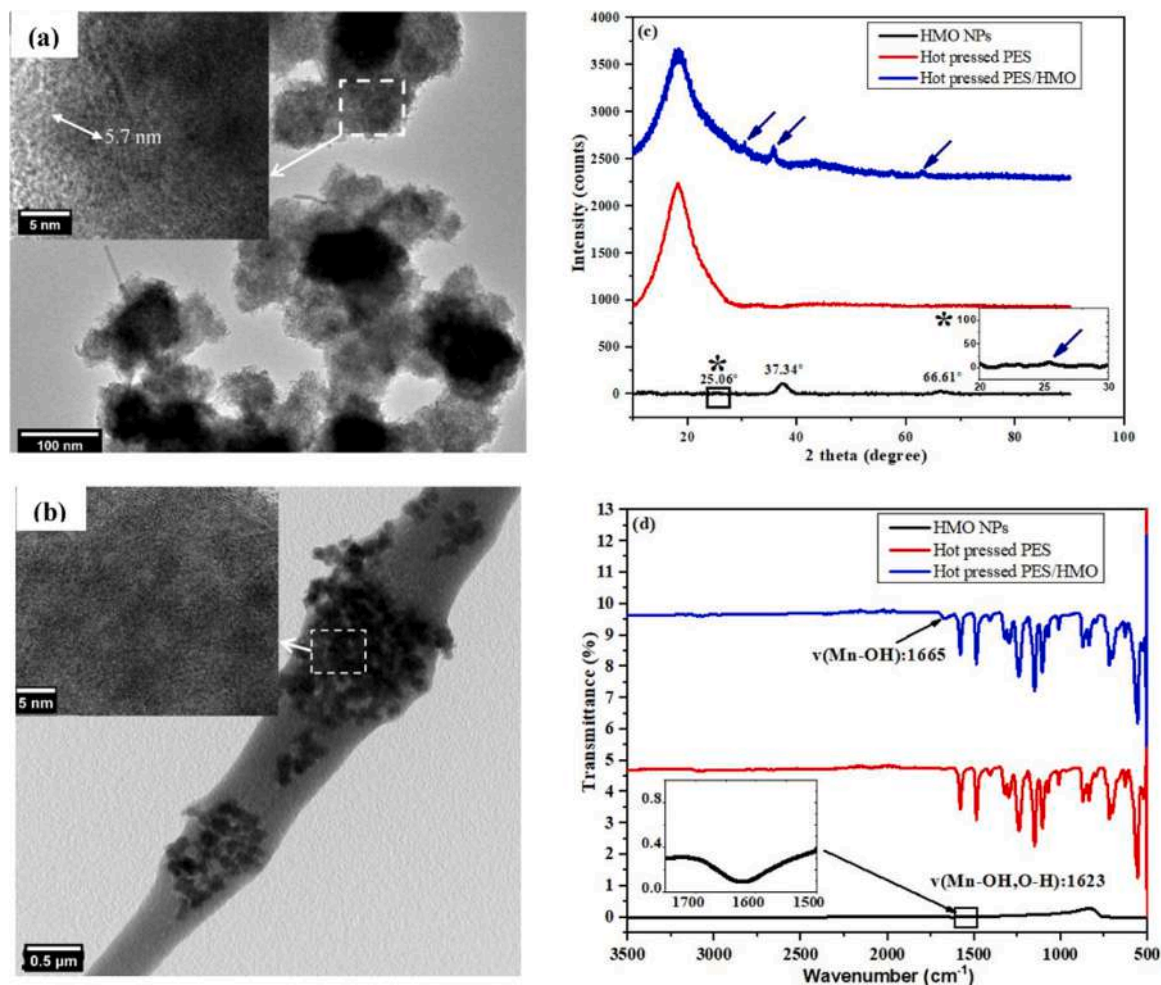


Fig. 5. HRTEM micrographs of the (a) HMO NPs, and (b) hot-pressed PES embedded with HMO (captured at different scales), (c) XRD micrographs and (d) FTIR spectra of the ENMs.

NPs [19,24–26]. Compared to hot-pressed PES membrane spectra, the Mn–OH band in the HMO NPs shifted to a higher wavenumber when they were incorporated into the PES membranes (Fig. 5(d)). This shift in Mn–OH band at approximately 1665 cm^{-1} relates to forming the organic-inorganic hybrid membrane. Moreover, the weak bands at 400 and 900 cm^{-1} disappeared when the HMO NPs were integrated into the polymeric matrix of the PES nanofibrous membrane. This result indicated that the HMO NPs were appropriately included in the membrane matrix with uniform dispersions. Moreover, no peaks were related to the chemical bonding between HMO NPs and PES, suggesting that the interaction is purely physical. Previous studies reported similar FTIR analysis results of pure PES and unmodified HMO [19,24–26].

3.1.3. Thermal properties

Fig. 6(a) displays the TGA curves of the ENM samples characterized by three mass loss stages: $30\text{--}100$, $100\text{--}200$ and $450\text{--}650\text{ }^{\circ}\text{C}$. The first ($30\text{--}100\text{ }^{\circ}\text{C}$), second ($100\text{--}200\text{ }^{\circ}\text{C}$) and third ($450\text{--}650\text{ }^{\circ}\text{C}$) mass loss stages are due to the evaporation of DMF on the polymer, the evaporation of NMP and other impurities, and the degradation of PES due to ether (C–O) bond cleavage, respectively. Overall, the nanofibrous membrane incorporated with HMO has better thermal behaviour than the unmodified membrane. Furthermore, the weight loss of the PES/HMO membrane was approximately 58.7% , which was lower than that of the PES membrane (63.4%). These results confirmed the positive impacts of HMO incorporation on ENM thermal stability.

3.1.4. Mechanical behaviour

The mechanical characteristics of the developed ENMs are provided in Table S2. Fig. 6(b) shows the mechanical behaviour, including the tensile strength (MPa) and the elongation at break (%), of the developed ENMs. As depicted in Fig. 6(b) and Table S2, the tensile properties of the PES/HMO nanofibrous membranes increased by 78.86% when compared to the hot-pressed PES nanofibrous membrane. Moreover, the elongation of the hot-pressed PES/HMO nanofibrous membranes at the breaking point was 0.50 ± 7.5 , which was 19.05% greater than that of the hot-pressed PES nanofibrous membrane (0.42 ± 2.1). Nevertheless, the increase in tensile strength of the PES/HMO nanofibrous membrane did not cause a loss of elongation, as demonstrated in Fig. 6(b). The significant improvement in the tensile property of the ENMs was due to the tightly connected chains in the hot-pressed PES (covalent bonds), whereby the chain sliding became difficult after adding a specific amount of HMO nanoparticles [33,40]. The shifting of Mn–OH bands towards high frequencies (FTIR spectra in Fig. 5(d)) indicates a strong hydrogen bond in the composite ENMs [37,41]. These results correlated with the other reports of Al-Husaini et al. [19] and Tijing et al. [37] regarding the nanocomposite ENMs' mechanical properties. Thus, the enhanced overall material properties of the PES/HMO nanocomposites can be attributed to the good interfacial interaction between HMO NPs and PES.

3.1.5. Hydrophilicity

Fig. 6(c) shows the mean WCA values for the produced ENMs. The

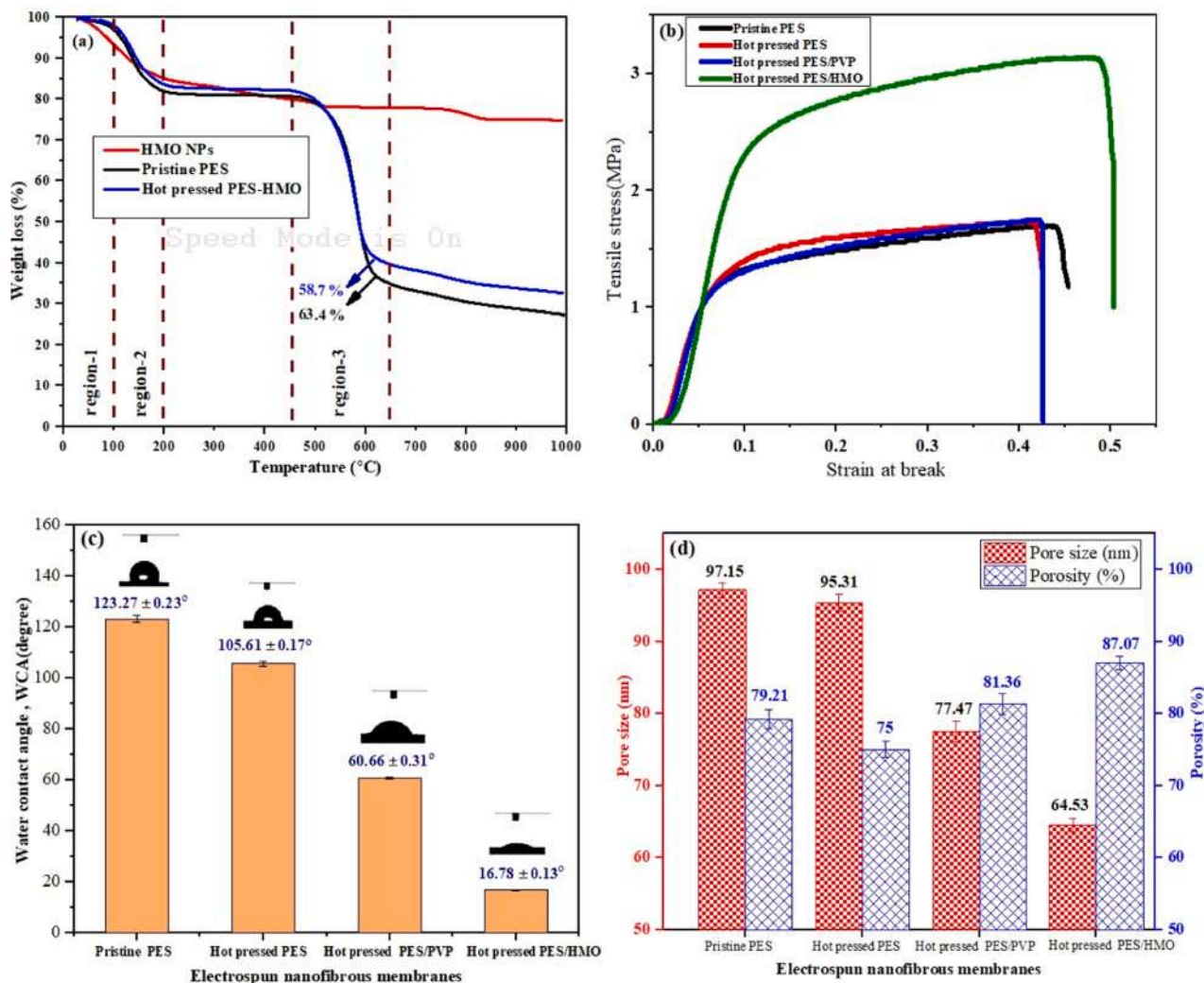


Fig. 6. Profile of the (a) TGA, (b) stress-strain curves, (c) measured WCA (together with image), and (d) pore size and the porosity of the fabricated ENMs.

hot-pressed PES/HMO ENMs had the highest hydrophilicity (i.e. 16.78°) among the ENMs (i.e. 123.27–60.66°). The hydrophilicity of the amorphous hydrous manganese dioxide can be attributed to the -OH groups (hydrophilic) on the membrane surface after HMO inclusion [24–26]. The superhydrophilicity of HMO NP (with an abundant amount of -OH functional groups) increased the affinity of the membrane toward water molecules, which remarkably reduced the WCA of the membrane surface [24]. The fouling mitigation also is reduced due to improved surface hydrophilicity hence allowing less frequency of membrane cleaning process [42]. However, PVP exerts less impact on the membrane surface hydrophilicity than the HMP NPs despite the hydrophilic nature of PVP because of the high solubility of PVP in the aqueous solution, in which most of the PVP leached out, especially during the storage of ENMs in the water solution. Table S3 shows the values of the measured WCA of the nanofibrous membranes in this study compared to those of previous studies [19,24–26,43]. Earlier studies demonstrated that better surface hydrophilicity of membranes has a positive impact on the minimization of the fouling that arises from the oil molecules (hydrophobic), and it reduces the degree of the membrane cleaning process. However, it is not easy to compare the result of this study to prior studies (see Table S3), as earlier studies had used different methods of nanofibrous membranes treatment and analysis. In addition, the CA depends not only on the surface hydrophilicity but also on many other factors such as surface roughness, porosities, pore sizes, and distribution of pore sizes [44,45].

3.1.6. Porosity and pore size distribution

As shown in Fig. 6(d), the porosity and pore size distribution of the synthesized ENMs were 75–87.07% and 64.53–97.15 nm, respectively. HPT decreased the porosity of the pristine PES ENM from 79.21% to 75% because of the reduction in fiber diameter. The voids between fibers decreased with increasing fiber network compactness [11,23]. However, the addition of hydrophilic components PVP and/or HMO NPs in the polymeric solution increased the porosity of the ENMs from 75% in the pristine PES ENMs to 81.36% and 87.07% in the hot-pressed PES/PVP and PES/HMO ENMs, respectively. This result can be ascribed to the fact that incorporating hydrophilic components in the PES-doped solution increased thermodynamic instability during electrospinning. This phenomenon affected the formation and orientation of the nanofibers [29,37]. The hot-pressed ENMs also had a lower pore size diameter (95.31 nm) than the pristine ENMs (97.15 nm) because of the fiber fusion during hot-pressing, which reduced porosity and pore size [23,27]. The incorporation of hydrophilic components PVP and/or HMO NP in the polymeric solution greatly reduced pore diameter (Fig. 6(d)). Specifically, the pore diameter decreased from 95.31 nm for the hot-pressed ENMs to 77.47 and 64.53 nm for the hot-pressed PES/PVP and PES/HMO ENMs, respectively. The viscosity (Table S1) and thermodynamic stability of the dope solution also changed when it was incorporated with the hydrophilic component, which altered the size of the pores and the porosity of ENMs [25,29,46]. Apart from that, the high porosity of membranes, particularly the PES/HMO membrane, is one of

the crucial factors contributing to the excellent water flux due to reducing water molecules' transport resistance [46,47]. Further discussions are provided below.

3.2. Filtration analysis of ENMs

3.2.1. Pure water flux evaluation before the oily treatment process (J_{w1})

Pure water fluxes of the fabricated ENMs were measured three times, and the mean values were obtained (Fig. 7(a)). The J_{w1} values of the

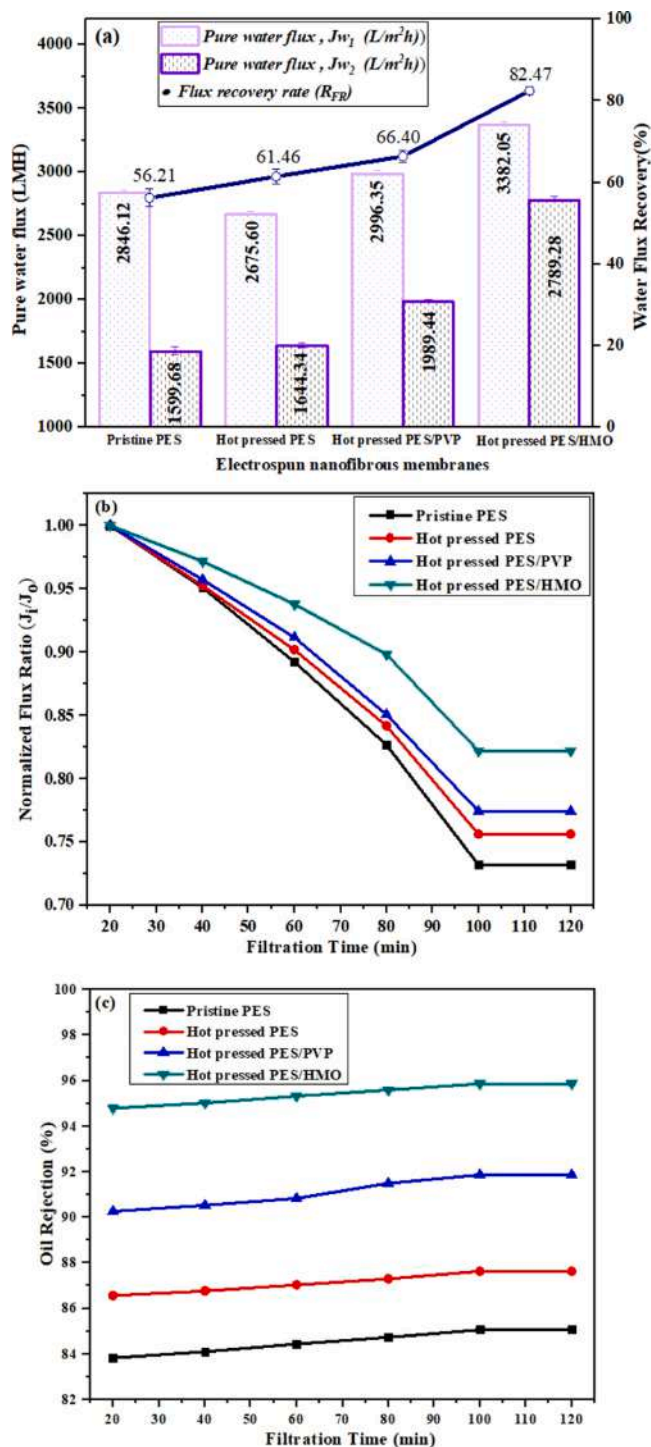


Fig. 7. Profiles of (a) mean pure water flux of ENMs before and after exposure to a synthetic oily solution, (b) normalized water flux and (c) oil rejection of ENMs when treated with 12,000 ppm oily solution.

ENMs were practically constant during the tests. However, HPT of the ENMs for 10 min to a temperature below the melting point at 1 bar significantly improved the adhesion of the fibers, which increased the flux, as reported by other studies [26,48]. In addition, the pristine ENM has a slightly higher flux (2846 ± 39.97 L/m²h) than the hot-pressed ENM (2675 ± 25.03 L/m²h) because of the high porosity of the pristine ENM. Other researchers reported similar observations [28,46], and the water flux primarily depended on membrane porosity [49]. The increase in membrane hydrophilicity also significantly improved the pure water flux of the hot-pressed PES/HMO nanofibrous membrane (Fig. 6(c)) together with structural modifications [1,28,50]. It is worth noting that membrane surface hydrophilicity is one of the important key players contributing to the enhancement of pure water flux [1,28]. In this study, the hydrophilicity is contributed by the existence of the affluent -OH groups in the HMO NPs. Using the van der Waals force, these functional groups could attract the water molecules easily onto the PES/HMO ENMs surface through hydrogen bonds, leading to an enhancement in the pure water flux and fouling resistance [25,37].

3.2.2. Sizes of emulsion droplets and permeate flux measurements

The distribution of oil droplet sizes in the synthetic oily mixture is shown in Fig. S3 (a). The estimated particle sizes were in the range of 58.8–95.4 nm with an average diameter of 286.4 ± 0.35 nm. In addition, Table S4 shows the physicochemical properties of the synthetic oily mixture samples, measured at room temperature. Moreover, Fig. 7(b) displays the normalized water flow performance of the ENMs produced as a function of operating time for the cross-flow UF experiment when treated with 12,000 ppm oil molecules in a synthetic oily solution. As shown in Fig. 7(b), the permeate flow of the nanofiber membranes was in the order hot-pressed PES/HMO > hot-pressed PES/PVP > hot-pressed PES > pure PES-ENMs. The permeate flow of the synthetic oil (12,000 ppm oil molecules) was considerably lower than that of the pure water flow, although these values agreed with the J_{w1} values shown earlier (Fig. 7(a)). This result can be ascribed to the formation of cake layer oil on the nanofiber membrane surface, which agrees with Lai et al. [26] and Gohari et al. [25]. As shown in Table S4, the formation of cake layer oil deteriorated with increasing feed solution viscosity, as reported by Al-Husaini et al. [19]. This phenomenon later strengthened the water transport resistance in the system and delayed any improvement in water flow, which concurred with Ong et al. [30]. As depicted in Fig. 7 (b), the flow of the pristine PES nanofiber membrane strongly deteriorated, in which the value of (J_t/J_0) decreased from 1.0 to 0.73 within the duration of the experiment (120 min). This decreased 27% compared to the corresponding water flow recorded initially. The water flow reductions of the hot-pressed PES, PES/PVP and PES/HMO ENMs were 24.3%, 22.65% and 17.7%, respectively. The excellent permeate flux and lowest flux declination of the hot-pressed PES/HMO nanofiber membrane were mainly contributed by improving the membrane morphology and surface hydrophilicity [19,25,32]. It is noteworthy that the ENMs thickness (by electrospinning time for 9 h by changing the flow rate every 3 h of duration) also played an essential role in the permeate flow during the separation process [27,49]. As shown in Table S4, these results prove that the physicochemical properties of oil droplets also, particularly oil droplet sizes play a vital role in controlling the permeate flow of the ENMs upon exposure to 12,000 ppm of synthetic oily solution [26,32]. Low permeate flux due to severe pore blockage could occur as some of the oil droplets (in the range of 24.4–58.8 nm) in the feed were smaller compared to the pore size of the PES/HMO ENMs (average size of 61.05 nm) [25,26,32]. Fouling (organic materials deposition on the membrane pores and surface) also decreased the permeation flux as a function of the ENM, as reported by Zularisam et al. [51].

3.2.3. Oil rejection measurements

Fig. 7(c) shows the operating time-dependent oil repellency of the ENMs when treated with an oily solution (12,000 ppm) within 2 h of the

test. Fig. S3 (b) shows the average efficiency of the oil separation of each nanofiber membrane when treated with an oily solution (12,000 ppm) within 2 h of the test. The hot-pressed PES/HMO-ENMs showed a significantly higher rejection (95.42%) than the other membranes throughout the test (Fig. S3 (b)). The qualities of the permeate samples were excellent and contained an insignificant amount of oil molecules which are difficult to distinguish with the naked eye. This result indicates that the membranes can achieve high separation efficiency by incorporating hydrophilic HMO-NPs into the PES-based membrane. It also contributed to two reasons that caused the high performance of the hot-pressed PES/HMO-ENMs. The first reason was the smaller pore sizes of the membrane surface (Fig. 6(d)) than the mean oil particles in the oily solution (Fig. S3 (a)). This phenomenon helped prevent the oil particles from passing through the membranes [25,52,53]. The second reason was the highest surface hydrophilicity of the PES/HMO ENM among the samples evaluated (Fig. 6(c)), which reduced oil deposition and/or absorption [23,25,26]. It was affirmed that the decrease in oil rejection of the ENMs in treating 12000 ppm oily solution was also affected by the membrane properties (particularly pore sizes) and oil droplet sizes. This is because some of the tiny oil droplets might permeate through the pores, reducing the oil rejection rate as experienced. Others have also observed similar observations [25,26,30,47,53].

3.2.4. Pure water flux evaluation after the oily treatment process

After the oil-water emulsion treatment, the nanofibrous membranes were cleaned, and the pure water flux (J_{w2}) of the ENMs was measured three times to examine the flux recovery ratio (R_{FR}). The average pure water fluxes (J_{w2}) of the ENMs after synthetic oily solution treatment are displayed in Fig. 7(a). The J_{w2} values of the hot-pressed PES/HMO ENMs decreased by 17.53% compared with their J_{w1} values (Fig. 7(a)) because of the high oil adhesion toward the solid surface [54]. Gohari et al. [25] stated that simple water cleaning was less effective for membrane cleaning due to the thicker oil layer formed on the membrane surface upon the filtration process. Masuelli [32] also found that only weakly adsorbed emulsion droplets can be easily removed by water, resulting in differences in J_{w2} values due to the modification of the surface/porous structure after washing with water. Meanwhile, Lai et al. [26] proved that the pure water flux of the nanofiller-included membranes was largely recovered after washing by simple rinsing with oily solution treatments. Therefore, the foulant accumulation on the hot-pressed PES/HMO nanofibrous membrane surface was less than that on the other developed membranes. In addition, the membrane had a smaller average pore size (Fig. 6(d)) than the oil particles in the oily solution (Fig. S3 (a)). When the hot-pressed PES/HMO ENMs were wet, the oil droplets could more easily be washed away than when they were dry. This disclosure can be attributed to the improved hydrophilicity of the ENMs. This hydrophilicity attracted more water molecules on the surface, weakening any direct interaction between oil droplets and the PES membranes [26]. Therefore, a simple rinsing with water showed that the pure water flux of the nanofiller-included membranes was largely recovered after oily solution treatments. Referring to Fig. 7(a), the hot-pressed PES/HMO nanofibrous membrane achieved the highest pure water flux before (J_{w1}) and after (J_{w2}) synthetic oily solution treatments among the fabricated ENMs. This result was primarily attributed to the enhanced morphologies of the membranes with a high degree of porosity and promising surface hydrophilicity [19,55].

3.2.5. Flux recovery rate (R_{FR})

The water flux recovery rate (R_{FR}) of the fabricated ENMs was evaluated and defined by Eq. (4) based on the ratio of pure water flux of ENMs before (J_{w1}) and after synthetic oily solution treatment (J_{w2}), as shown in Fig. 7(a). The optimum water flux recovery rate ($82.47\% \pm 0.90\%$) was achieved by the hot-pressed PES/HMO ENMs, followed by the hot-pressed PES/PVP ($66.40\% \pm 1.4\%$), hot-pressed PES ($61.46\% \pm 1.9\%$) and pristine PES ($56.21\% \pm 2.2\%$) membranes. During fouling, emulsion droplets are deposited on the membrane surfaces

and pores by the interactions between the ENMs and the emulsions. This phenomenon can strengthen resistance to the outer flow through the membrane, thereby decreasing the permeate flux and strongly affecting the water flux recovery [25,26,56,57]. The hydrophilicity of the hot-pressed PES/HMO ENMs sufficiently weakened the interaction between the oily substances and the ENM surface, which increased the recovery rate. This correlation can be observed with a higher $J_{w2}:J_{w1}$ ratio and was acknowledged by Lai et al. [26] and Salimi et al. [35]. The high-performance recovery rate can ensure the long lifespan of the membranes and low cleaning rates. Nevertheless, the high recovery ratio (J_{w2}/J_{w1}) of the hot-pressed PES/HMO ENMs also indicates that the hot-pressed PES/HMO membrane was prepared using an oily feed solution at 12,000 ppm. The present study can be used as a reference for treating the oily solution discharged from industries without severe flux declination, considering that the oil contents of industrial effluents are usually within 100–800 ppm (depending on the physicochemical characteristics of the oily solution discharged) [25]. Thus, the hydrophilic HMO NPs can strengthen the hydrophilicity of the membrane and weaken the interaction between the hydrophobic oil droplets and the membrane surface during oily wastewater treatment. Therefore, among the membranes studied, the hot-pressed PES/HMO nanofibrous membrane performs best among the four ENMs in terms of water permeability, oil rejection and recovery ratio (J_{w2}/J_{w1}).

Table S3 compares the performance of the PES-based UF membranes incorporated with HMO NPs synthesized in this work with other recently published works for oily solution treatment with respect to water flux, oil rejection rate, and flux recovery properties. Nevertheless, it is evident from the data summarized in the Table S3, the newly synthesized HMO-incorporated PES ENMs have a great potential to separate oil molecules from highly concentrated oily solutions by achieving a higher combination of water flux and oil rejection rate compared to the relevant published works in the literature. Although many previous works have reported the complete elimination of oil molecules from the synthesized solutions, the concentrations of the feed solution used were much lower compared to our current work. For instance, Gohari et al. [25] reported almost 100% oil rejection using a PES membrane modified by hydrophilic HMO NPs, but the feed concentration was only 1000 ppm. There are some works that investigated the performance of polymeric membranes for oily solutions with 5000–10000 ppm concentration [19,58], but oil concentrations up to 12000 ppm are rarely found in the literature. Recently, Al-Husaini et al. [19] reported 94.04% rejection and a promising 71.10% flux recovery of the PES HMO ENMs using a feed solution containing 10000 ppm oil molecules. However, the feed solution concentration used was lower compared to our current work. Although Doraisammy et al. [43] evaluated the performance of the PES incorporated with HMO NPs using a higher oily solution concentration (up to 15000 ppm), its rate of oil rejection was still significantly lower than those tested in this work. The fact that some previous authors had used different membrane materials or different methods of nanofibrous membranes treatment and analysis makes it difficult to compare the results of this study with previous studies (see Table S3). Furthermore, the membrane separation performance is influenced by concentrations of the feed solution used and the differences in oily solution properties (e.g. average particle size and type of oil). This is because the membranes used for highly concentrated oily solution treatment tend to deteriorate quickly and experience severe fouling within a short period, unlike the oily solutions with low concentration, as reported by Doraisammy et al. [43] and Zulkefli et al. [44]. Thus, these results confirm the better performance of HMO-incorporated PES ENMs for the treatment of highly concentrated oily solutions for long-standing operations with extreme durability.

4. Conclusions

This paper has demonstrated novel PES ENMs incorporated with hydrophilic HMO NPs for enhanced UF of the oily solution. The PES

ENMs were fabricated by adding HMO NPs into the dope solution composed of DMF/NMP mixed solvents followed by heat treatment (on the resultant membranes) to improve their properties. FESEM images proved that the average PES ENMs diameter and thickness decreased remarkably from 421 to 179 nm and 268–231 μm , respectively, by incorporating HMO NPs and hot pressing treatment. The best promising HMO NP-incorporated ENMs exhibited higher water flux (3382 $\text{L}/\text{m}^2\cdot\text{h}$) and lower fouling propensity than the pristine PES ENM (2846 $\text{L}/\text{m}^2\cdot\text{h}$). In addition, the tensile strength improved significantly compared to the pristine PES ENMs, which also exhibited the lowest WCA (16.78°) with the highest porosity (87.07%). The results revealed that the ENMs incorporated with HMO NPs exhibited excellent oil rejection (95.42%) and promising water flux recovery (82.47%) upon exposure to a synthetic oily solution (12,000 ppm). It must be noted that the promising water flux achieved by the developed PES/HMO ENM did not compromise its oil rejection rates as the membrane was still able to produce permeate of high quality after exposure to an oily solution (12,000 ppm). Such characteristics were attributed to its super-hydrophilic HMO NPs, which modified ENMs morphology. This study revealed the potential of using HMO nanoparticles as an alternative filler in improving the properties of PES ENMs, making them suitable for use in environmental remediation specifically for treating oily wastewater.

CRedit authorship contribution statement

Dr. Issa Sulaiman Al-Husaini: Supervision for the project leading to this publication. Conceptualization, methodology, formal analysis, Origin software (graphing and data analysis software), formal analysis, and writing-original draft preparation. **Prof. Dr. Abdull Rahim Mohd Yusoff:** Editing and financial support for the project leading to this publication. **Dr. Mohd Dzul Hakim Wirzal:** Methodology, validation, resources, writing-reviewing, and editing.

Declaration of Competing Interest

The authors declare that they have no known competing financial interests or personal relationships that could have appeared to influence the work reported in this paper.

Data availability

No data was used for the research described in the article.

Acknowledgments

The authors would like to thank the Chemistry Department (Faculty of Science, Universiti Teknologi Malaysia, Malaysia) and Nanotechnology Research Centre (Sultan Qaboos University, Oman) for providing assistance and facilities for this project completion.

Appendix A. Supporting information

Supplementary data associated with this article can be found in the online version at [doi:10.1016/j.jece.2022.108341](https://doi.org/10.1016/j.jece.2022.108341).

References

- [1] P. Arribas, M. García-Payo, M. Khayet, L. Gil, Heat-treated optimized polysulfone electrospun nanofibrous membranes for high performance wastewater microfiltration, *Sep. Purif. Technol.* 226 (2019) 323–336, <https://doi.org/10.1016/j.seppur.2019.05.097>.
- [2] S. Ahmadipouya, S.A. Mousavi, A. Shokrgozar, D.V. Mousavi, Improving dye removal and antifouling performance of polysulfone nanofiltration membranes by incorporation of ui0-66 metal-organic framework, *J. Environ. Chem. Eng.* 10 (3) (2022), 107535, <https://doi.org/10.1016/j.jece.2022.107535>.
- [3] I.S. Al-Husaini, A.R. Yusoff, W.J. Lau, A.F. Ismail, and M.Z. Al-Abri, Nanofiber membranes for oily wastewater treatment, in nanofiber membranes for medical, Environmental, and Energy Applications, Ahmad Fauzi Ismail, Nidal Hilal, Juhana

- Jaafar, and C. J. Wright, Editors. (2019), CRC Press: Boca Raton. <https://doi.org/10.1201/9781351174046>.
- [4] R. Gopal, S. Kaur, C.Y. Feng, C. Chan, S. Ramakrishna, S. Tabe, T. Matsuura, Electrospun nanofibrous polysulfone membranes as pre-filters: Particulate removal, *J. Membr. Sci.* 289 (1–2) (2007) 210–219, <https://doi.org/10.1016/j.memsci.2006.11.056>.
- [5] I.S. Al-Husaini, K. Sakthipandi, Improvements in electrospun nanofibrous membranes and their applications in water treatments, *J. Appl. Mem. Sci. Technol.* 24 (3) (2020) 31–56.
- [6] N.S. Abd Halim, M.D.H. Wirzal, M.R. Bilad, N.A.H. Md Nordin, Z. Adi Putra, N. S. Sambudi, A.R. Mohd Yusoff, Improving performance of electrospun nylon 6, 6 nanofiber membrane for produced water filtration via solvent vapor treatment, *Polym* 11 (12) (2019) 2117, <https://doi.org/10.3390/polym11122117>.
- [7] C.Y. Foong, M.F.M. Zulkifli, M.D.H. Wirzal, M.A. Bustam, L.H.M. Nor, M.S. Saad, N. S. Abd Halim, COSMO-RS prediction and experimental investigation of amino acid ionic liquid-based deep eutectic solvents for copper removal, *J. Mol. Liq.* 333 (2021), 115884, <https://doi.org/10.1016/j.molliq.2021.115884>.
- [8] M.S. Saad, L. Balasubramaniam, M.D.H. Wirzal, N.S. Abd Halim, M.R. Bilad, N.A. H. Md Nordin, Z. Adi Putra, F.N. Ramli, Integrated membrane-electrocoagulation system for removal of celestine blue dyes in wastewater, *Membr* 10 (8) (2020) 184, <https://doi.org/10.3390/membranes10080184>.
- [9] P. Arribas, M. Khayet, M. Garcia-Payo, L. Gil, Self-sustained electro-spun polysulfone nano-fibrous membranes and their surface modification by interfacial polymerization for micro-and ultra-filtration, *Sep. Purif. Technol.* 138 (2014) 118–129, <https://doi.org/10.1016/j.seppur.2014.10.010>.
- [10] Y. Liu, R. Wang, H. Ma, B.S. Hsiao, B. Chu, High-flux microfiltration filters based on electrospun polyvinylalcohol nanofibrous membranes, *Polymer* 54 (2) (2013) 548–556, <https://doi.org/10.1016/j.polymer.2012.11.064>.
- [11] I.S. Al-Husaini, W.-J. Lau, A.R.M. Yusoff, M.Z. Al-Abri, B.A. Al Farsi, Synthesis of functional hydrophilic polyethersulfone-based electrospun nanofibrous membranes for water treatment, *J. Environ. Chem. Eng.* 9 (1) (2021), 104728, <https://doi.org/10.1016/j.jece.2020.104728>.
- [12] X. Yin, Z. Zhang, H. Ma, S. Venkateswaran, B.S. Hsiao, Ultra-fine electrospun nanofibrous membranes for multicomponent wastewater treatment: Filtration and adsorption, *Sep. Purif. Technol.* 242 (2020), 116794, <https://doi.org/10.1016/j.seppur.2020.116794>.
- [13] D. Bjorge, N. Daels, S. De Vrieze, P. Dejans, T. Van Camp, W. Audenaert, J. Hogue, P. Westbroek, K. De Clerck, S.W. Van Hulle, Performance assessment of electrospun nanofibers for filter applications, *Desalin* 249 (3) (2009) 942–948, <https://doi.org/10.1016/j.desal.2009.06.064>.
- [14] N. Yang, X. Wen, T.D. Waite, X. Wang, X. Huang, Natural organic matter fouling of microfiltration membranes: prediction of constant flux behavior from constant pressure materials properties determination, *J. Membr. Sci.* 366 (1–2) (2011) 192–202, <https://doi.org/10.1016/j.memsci.2010.10.003>.
- [15] Q. Wang, Y. Bai, J. Xie, Q. Jiang, Y. Qiu, Synthesis and filtration properties of polyimide nanofiber membrane/carbon woven fabric sandwiched hot gas filters for removal of PM 2.5 particles, *Powder Technol.* 292 (2016) 54–63, <https://doi.org/10.1016/j.powtec.2016.01.008>.
- [16] J. Bae, I. Baek, H. Choi, Mechanically enhanced PES electrospun nanofiber membranes (ENMs) for microfiltration: The effects of ENM properties on membrane performance, *Water Res* 105 (2016) 406–412, <https://doi.org/10.1016/j.watres.2016.09.020>.
- [17] L. Huang, J.T. Arena, S.S. Manickam, X. Jiang, B.G. Willis, J.R. McCutcheon, Improved mechanical properties and hydrophilicity of electrospun nanofiber membranes for filtration applications by dopamine modification, *J. Membr. Sci.* 460 (2014) 241–249, <https://doi.org/10.1016/j.memsci.2014.01.045>.
- [18] L. Huang, S.S. Manickam, J.R. McCutcheon, Increasing strength of electrospun nanofiber membranes for water filtration using solvent vapor, *J. Membr. Sci.* 436 (2013) 213–220, <https://doi.org/10.1016/j.memsci.2012.12.037>.
- [19] I.S. Al-Husaini, A. Yusoff, W. Lau, A. Ismail, M. Al-Abri, B. Al-Ghafri, M. Wirzal, Fabrication of polyethersulfone electrospun nanofibrous membranes incorporated with hydrous manganese dioxide for enhanced ultrafiltration of oily solution, *Sep. Purif. Technol.* 212 (2019) 205–214, <https://doi.org/10.1016/j.seppur.2018.10.059>.
- [20] R. Gopal, S. Kaur, Z. Ma, C. Chan, S. Ramakrishna, T. Matsuura, Electrospun nanofibrous filtration membrane, *J. Membr. Sci.* 281 (1–2) (2006) 581–586, <https://doi.org/10.1016/j.memsci.2006.04.026>.
- [21] M.T.M. Pendergast, J.M. Nygaard, A.K. Ghosh, E.M. Hoek, Using nanocomposite materials technology to understand and control reverse osmosis membrane compaction, *Desalin* 261 (3) (2010) 255–263, <https://doi.org/10.1016/j.desal.2010.06.008>.
- [22] S.A. Hosseini, M. Vossoughi, N.M. Mahmoodi, M. Sadrzadeh, Efficient dye removal from aqueous solution by high-performance electrospun nanofibrous membranes through incorporation of SiO₂ nanoparticles, *J. Clean. Prod.* 183 (2018) 1197–1206, <https://doi.org/10.1016/j.jclepro.2018.02.168>.
- [23] I.S. Al-Husaini, A.R.M. Yusoff, W.-J. Lau, A.F. Ismail, M.Z. Al-Abri, M.D.H. Wirzal, Iron oxide nanoparticles incorporated polyethersulfone electrospun nanofibrous membranes for effective oil removal, *Chem. Eng. Res. Des.* 148 (2019) 142–154, <https://doi.org/10.1016/j.cherd.2019.06.006>.
- [24] N. Ismail, W. Salleh, N. Awang, S. Ahmad, N. Rosman, N. Szali, A. Ismail, PVDF/HMO ultrafiltration membrane for efficient oil/water separation, *Chem. Eng. Commun.* 208 (4) (2021) 463–473, <https://doi.org/10.1080/00986445.2019.1650035>.
- [25] R.J. Gohari, E. Halakoo, W. Lau, M. Kassim, T. Matsuura, A. Ismail, Novel polyethersulfone (PES)/hydrous manganese dioxide (HMO) mixed matrix membranes with improved anti-fouling properties for oily wastewater treatment

- process, RSC Adv. 4 (34) (2014) 17587–17596, <https://doi.org/10.1039/C4RA00032C>.
- [26] G. Lai, M. Yusob, W. Lau, R.J. Gohari, D. Emadzadeh, A. Ismail, P. Goh, A. Isloor, M.R.-D. Arzhandi, Novel mixed matrix membranes incorporated with dual-nanofillers for enhanced oil-water separation, Sep. Purif. Technol. 178 (2017) 113–121, <https://doi.org/10.1016/j.seppur.2017.01.033>.
- [27] S.S. Homaeigohar, K. Buhr, K. Ebert, Polyethersulfone electrospun nanofibrous composite membrane form liquid filtration, J. Membr. Sci. 365 (1–2) (2010) 68–77, <https://doi.org/10.1016/j.memsci.2010.08.041>.
- [28] K. Yoon, B.S. Hsiao, B. Chu, Formation of functional polyethersulfone electrospun membrane for water purification by mixed solvent and oxidation processes, Polym 50 (13) (2009) 2893–2899, <https://doi.org/10.1016/j.polymer.2009.04.047>.
- [29] N. Nor, J. Jaafar, A. Ismail, M.A. Mohamed, M. Rahman, M.H. Othman, W.J. Lau, N. Yusof, Preparation and performance of PVDF-based nanocomposite membrane consisting of TiO₂ nanofibers for organic pollutant decomposition in wastewater under UV irradiation, Desalin 391 (2016) 89–97, <https://doi.org/10.1016/j.desal.2016.01.015>.
- [30] C. Ong, W. Lau, P. Goh, B. Ng, A. Ismail, Preparation and characterization of PVDF-PVP-TiO₂ composite hollow fiber membranes for oily wastewater treatment using submerged membrane system, Desalin. Water Treat. 53 (5) (2015) 1213–1223, <https://doi.org/10.1080/19443994.2013.855679>.
- [31] Y. Liu, X. Yue, S. Zhang, J. Ren, L. Yang, Q. Wang, G. Wang, Synthesis of sulfonated polyphenylsulfone as candidates for antifouling ultrafiltration membrane, Sep. Purif. Technol. 98 (2012) 298–307, <https://doi.org/10.1016/j.seppur.2012.06.031>.
- [32] M.A. Masuelli, Ultrafiltration of oil/water emulsions using PVDF/PC blend membranes, Desalin. Water Treat. 53 (3) (2015) 569–578, <https://doi.org/10.1080/19443994.2013.846539>.
- [33] F.E. Ahmed, B.S. Lalia, N. Hilal, R. Hashaikheh, Underwater superoleophobic cellulose/electrospun PVDF-HFP membranes for efficient oil/water separation, Desalin 344 (2014) 48–54, <https://doi.org/10.1016/j.desal.2014.03.010>.
- [34] B.Y.L. Tan, J. Juay, Z. Liu, D. Sun, Flexible hierarchical TiO₂/Fe₂O₃ composite membrane with high separation efficiency for surfactant-stabilized oil-water emulsions, Asian J. Chem. 11 (4) (2016) 561–567, <https://doi.org/10.1002/asia.201501203>.
- [35] E. Salimi, A. Ghaee, A.F. Ismail, Performance and antifouling enhancement of polyethersulfone hollow fiber membranes incorporated with highly hydrophilic hydroxyapatite nanoparticles, RSC Adv. 6 (50) (2016) 44480–44488, <https://doi.org/10.1039/C6RA05451J>.
- [36] B. Kwankhao, Microfiltration membranes via electrospinning of polyethersulfone solutions. (2013), Duisburg, Essen. 2013: Duisburg, Essen. <https://nbn-resolving.org/urn:nbn:de:hbz:464-20131213-102318-1>.
- [37] L.D. Tijing, W. Choi, Z. Jiang, A. Amarjargal, C.-H. Park, H.R. Pant, I.-T. Im, C. S. Kim, Two-nozzle electrospinning of (MWNT/PU)/PU nanofibrous composite mat with improved mechanical and thermal properties, Curr. Appl. Phys. 13 (7) (2013) 1247–1255, <https://doi.org/10.1016/j.cap.2013.03.023>.
- [38] H.R. Barai, A.N. Banerjee, S.W. Joo, Improved electrochemical properties of highly porous amorphous manganese oxide nanoparticles with crystalline edges for superior supercapacitors, J. Ind. Eng. Chem. 56 (2017) 212–224, <https://doi.org/10.1016/j.jiec.2017.07.014>.
- [39] S. Wan, M. Ma, L. Lv, L. Qian, S. Xu, Y. Xue, Z. Ma, Selective capture of thallium (I) ion from aqueous solutions by amorphous hydrous manganese dioxide, Chem. Eng. J. 239 (2014) 200–206, <https://doi.org/10.1016/j.cej.2013.11.010>.
- [40] S. Huang, L. Zhou, M.-C. Li, Q. Wu, Y. Kojima, D. Zhou, Preparation and properties of electrospun poly (vinyl pyrrolidone)/cellulose nanocrystal/silver nanoparticle composite fibers, Langmuir 9 (7) (2016) 523, <https://doi.org/10.3390/ma9070523>.
- [41] A. Martos, M. Herrero, A. Vázquez, B. Levenfeld, Synthesis and characterization of new membranes based on sulfonated polysulfone/Zn, Al-heptamolibdate LDH, Mater. Lett. 152 (2015) 125–127, <https://doi.org/10.1016/j.matlet.2015.03.094>.
- [42] S.N.W. Ikhsan, N. Yusof, F. Aziz, N. Misdan, A.F. Ismail, W.-J. Lau, J. Jaafar, W.N. W. Salleh, N.H.H. Hairom, Efficient separation of oily wastewater using polyethersulfone mixed matrix membrane incorporated with halloysite nanotube-hydrous ferric oxide nanoparticle, Sep. Purif. Technol. 199 (2018) 161–169, <https://doi.org/10.1016/j.seppur.2018.01.028>.
- [43] V. Doraisamy, G.S. Lai, S. Kartohardjono, W.J. Lau, K.C. Chong, S.O. Lai, H. Hasbullah, A.F. Ismail, Synthesis and characterization of mixed matrix membranes incorporated with hydrous manganese oxide nanoparticles for highly concentrated oily solution treatment, Can. J. Chem. Eng. 96 (2018) 1612–1619, <https://doi.org/10.1002/cjce.23092>.
- [44] N.F. Zulkefli, N.H. Alias, N.S. Jamaluddin, N. Abdullah, S.F. Abdul Manaf, N. H. Othman, F. Marpani, M.S. Mat-Shayuti, T.D. Kusworo, Recent mitigation strategies on membrane fouling for oily wastewater treatment, Membr 12 (2022) 26, <https://doi.org/10.3390/membranes12010026>.
- [45] N.U. Barambu, M.R. Bilad, M.A. Bustam, K.A. Kurnia, M.H.D. Othman, N.A.H. M. Nordin, Development of membrane material for oily wastewater treatment: a review, Ain Shams Eng. J. 12 (2021) 1361–1374, <https://doi.org/10.1016/j.asej.2020.08.027>.
- [46] S.P. Sundaran, C. Reshmi, A. Sujith, Tailored design of polyurethane based fouling-tolerant nanofibrous membrane for water treatment, New J. Chem. 42 (3) (2018) 1958–1972, <https://doi.org/10.1039/C7NJ03997B>.
- [47] C. Zhang, P. Li, B. Cao, Electrospun microfibrillar membranes based on PIM-1/POSS with high oil wettability for separation of oil-water mixtures and cleanup of oil soluble contaminants, Ind. Eng. Chem. Res 54 (35) (2015) 8772–8781, <https://pubs.acs.org/doi/abs/10.1021/acs.iecr.5b02321>.
- [48] L.T.S. Choong, Application of electrospun fiber membranes in water purification, Mass Inst. Technol; (2015). (<https://dspace.mit.edu/handle/1721.1/98153>).
- [49] W. Panatdasirisuk, Z. Liao, T. Vongsetskul, S. Yang, Separation of oil-in-water emulsions using hydrophilic electrospun membranes with anisotropic pores, Langmuir 33 (23) (2017) 5872–5878, <https://pubs.acs.org/doi/abs/10.1021/acs.langmuir.7b01138>.
- [50] A. Bokhary, M. Leitch, B. Liao, Effect of organic loading rates on the membrane performance of a thermophilic submerged anaerobic membrane bioreactor for primary sludge treatment from a pulp and paper mill, J. Environ. Chem. Eng. 10 (3) (2022), 107523, <https://doi.org/10.1016/j.jece.2022.107523>.
- [51] A. Zularisam, A. Ismail, R. Salim, Behaviours of natural organic matter in membrane filtration for surface water treatment—a review, Desalin 194 (1–3) (2006) 211–231, <https://doi.org/10.1016/j.desal.2005.10.030>.
- [52] A.K. Shukla, J. Alam, M. Alhoshan, L.A. Dass, M. Muthumareeswaran, Development of a nanocomposite ultrafiltration membrane based on polyphenylsulfone blended with graphene oxide, Sci. Rep. 7 (1) (2017) 1–12, <https://doi.org/10.1038/srep41976>.
- [53] H.C. Bidsorkhi, H. Riazi, D. Emadzadeh, M. Ghanbari, T. Matsuura, W. Lau, A. Ismail, Preparation and characterization of a novel highly hydrophilic and antifouling polysulfone/nanoporous TiO₂ nanocomposite membrane, Nanotechnol 27 (41) (2016), 415706, <https://doi.org/10.1088/0957-4484/27/41/415706>.
- [54] M.H. Tai, P. Gao, B.Y.L. Tan, D.D. Sun, J.O. Leckie, A hierarchically-nano structured TiO₂-carbon nanofibrous membrane for concurrent gravity-driven oil-water separation, Int. J. Environ. Sci. 6 (8) (2015) 590, <https://doi.org/10.7763/IJESD.2015.V6.663>.
- [55] B. Bolto, J. Zhang, X. Wu, Z. Xie, A review on current development of membranes for oil removal from wastewaters, Membr 10 (4) (2020) 65, <https://doi.org/10.3390/membranes10040065>.
- [56] N.S. Abd Halim, M.D.H. Wirzal, S.M. Hizam, M.R. Bilad, N.A.H.M. Nordin, N. S. Sambudi, Z.A. Putra, A.R.M. Yusoff, Recent development on electrospun nanofiber membrane for produced water treatment: a review, J. Environ. Chem. Eng. 9 (1) (2021), 104613 <https://doi.org/10.1016/j.jece.2020.104613>.
- [57] M. Safarpour, S. Najjarizad-Peyvasti, A. Khataee, A. Karimi, Polyethersulfone ultrafiltration membranes incorporated with CeO₂/GO nanocomposite for enhanced fouling resistance and dye separation, J. Environ. Chem. Eng. 10 (3) (2022), 107533, <https://doi.org/10.1016/j.jece.2022.107533>.
- [58] S. Elhady, M. Bassyouni, R.A. Mansour, M.H. Elzahar, S. Abdel-Hamid, Y. Elhenawy, M.Y. Saleh, Oily wastewater treatment using polyamide thin film composite membrane technology, Membr 10 (2020) 84, <https://doi.org/10.3390/membranes100500834>.